Sustainable Materials and Technologies 34 (2022) e00519

Contents lists available at ScienceDirect

Sustainable Materials and Technologies

journal homepage: www.elsevier.com/locate/susmat

Sustainable strategies for waterborne electrospinning of biocompatible nanofibers based on soy protein isolate

Mai Bay Stie [a,b,1], Kleopatra Kalouta [a,b,d,1], Cristiana Filipa Barreiro da Cunha [a,b], Halimah Masood Feroze [a], Valeria Vetri [c,**], Vito Foderà [a,b,*]

[a] Department of Pharmacy, University of Copenhagen, Universitetsparken 2, 2100 Copenhagen, Denmark
[b] Center for Biopharmaceuticals and Biobarriers in Drug Delivery, University of Copenhagen, Universitetsparken 2, 2100 Copenhagen, Denmark
[c] Dipartimento di Fisica e Chimica, Università Degli Studi di Palermo, Viale delle Scienze ed. 18, 90128 Palermo, Italy
[d] Dipartimento di Scienze e Tecnologie Biologiche Chimiche e Farmaceutiche (STEBICEF), Università Degli Studi di Palermo, Viale delle Scienze ed. 16, 90128 Palermo, Italy

ARTICLE INFO

Keywords:
Soy protein isolate
Electrospinning
Waterborne
Sustainable
Green materials

ABSTRACT

Electrospun nanofibers have gained great interest in many fields of research from water and air filtration or food packaging to medical use as scaffolds for tissue engineering, drug delivery systems and wound bandages. Proteins such as soy protein isolate (SPI) are biodegradable and safe polymers that can be purified from renewable and sustainable sources, and are thus interesting as building blocks for sustainable and biocompatible nanofiber-based materials. Sufficient solvent evaporation and intermolecular entanglement are required for efficient nanofiber formation. Electrospinning of proteins is therefore often achieved using organic solvents, strong bases or surfactants, which limits the safety, sustainability and usability of protein-based nanofibers. In this work, green and biocompatible electrospun nanofibers with a high content of SPI (up to 75% (w/w)) were fabricated with polyethylene oxide (PEO) as a *co*-spinning polymer and with water being the only solvent, thus avoiding use of any organic solvent, strong base or surfactant. A thorough biophysical assessment based on microscopy and spectroscopies, and a rheological profiling of SPI suggested that disassembly of larger structures into smaller in the SPI suspension and increase of SPI solubility improved the electrospinnability of SPI. The content of SPI in the nanofibers affected the morphology as visualized by scanning electron microscopy, brittleness assessed by dynamic mechanical analysis, and aqueous stability of the nanofibers, which are key parameters for the future use of SPI-based nanofibers. The biocompatibility of the electrospun SPI/PEO nanofibers was demonstrated by exposure of human epithelial cell monolayers (TR146) to the nanofibers without loss of cell viability. We propose that the presented strategies can serve as a universal workflow for waterborne electrospinning of other proteins or protein isolates.

1. Introduction

The current environmental status raises awareness for more eco-friendly and safe manufacturing technologies and a circular bio-economy [1]. Hence, currently, green manufacturing of sustainable materials is in focus to relieve the environmental burden caused by material fabrication. Proteins are naturally derived polymers that can be purified from renewable sources, are biodegradable and safe because of their natural origin and can in many cases partially or completely substitute synthetic polymers [2,3]. In general proteins of plant origin benefit from being cost-effective and a safe solution for those who avoid consuming animal-based products, and are not associated with animal-borne diseases [4,5]. Indeed, the use of proteins as building blocks for the fabrication of new biomaterials is intriguing as proteins are versatile, abundant in nature and sustainable [6]. Many types of materials including films [2,7,8], hydrogels [9–11] and nanofibers [12,13] have been successfully made from proteins. Nevertheless, the broad use of proteins as constituents of biomaterials often possesses significant

* Corresponding author at: Department of Pharmacy, University of Copenhagen, Universitetsparken 2, 2100 Copenhagen, Denmark.
** Corresponding author at: Dipartimento di Fisica e Chimica, Università Degli Studi di Palermo, Viale delle Scienze ed. 18, 90128 Palermo, Italy.
E-mail addresses: valeria.vetri@unipa.it (V. Vetri), vito.fodera@sund.ku.dk (V. Foderà).
[1] Shared first author.

https://doi.org/10.1016/j.susmat.2022.e00519
Received 4 May 2022; Received in revised form 21 October 2022; Accepted 6 November 2022
Available online 11 November 2022

challenges, such as poor mechanical properties and poor solubility, which must be overcome for the widespread use of protein-based biomaterials.

Electrospun nanofibers have gained a great interest as a material for applications in many areas from textile production [14,15], air [16] and water [17] filtration or food packaging [18] to medical use as scaffolds for tissue engineering [19], as drug delivery systems [13,20] and wound bandages [21]. Nanofiber fabrication by electrospinning is facilitated by an external electrical field that drives the formation of thin dry fibers by intermolecular entanglement in solution and efficient evaporation of the solvent during the process [22]. Efficient solvent evaporation is crucial for the formation of nanofibers without artifacts such as beading, which has led many types of polymers, both of natural and synthetic origin, to be electrospun in the presence of volatile organic solvents [22,23]. Similar protocols are applied for electrospinning of proteins, and solvents such as hexafluoro-2-propanol (HFIP) and formic acid have often been used to facilitate electrospinning of proteins and protein isolates [12,23]. However, the use of certain organic solvents can significantly compromise the sustainability of materials made of electrospun nanofibers, but also the biocompatibility and safety of the nanofibers, which can limit their future use [24]. In contrast, electrospinning from an aqueous solution, also called waterborne electrospinning [13,25], is per se the most environmentally friendly and safe form of electrospinning as the use of organic solvents is completely avoided. However, waterborne electrospinning can be challenging as water has a higher boiling point than the organic solvents often used to improve solvent evaporation during the electrospinning process. Furthermore, some proteins display low solubility and low intermolecular entanglement in aqueous solutions, which can make it difficult to fabricate nanofibers based on those proteins by the electrospinning technique [26,27].

Soy protein isolate (SPI) is a plant-based extract from soybean with a protein content of ≥90%, is one of the most abundant isolates available, and is derived as a side product of the soybean oil production industry [28]. The trimer, glycoprotein β-conglycinin (7S, Mw 150–200 kDa) and the hexamer glycinin (11S, Mw 300–380 kDa) are the two major protein fractions of SPI [29]. SPI-based nanofibers were shown to support wound healing and inhibit bacterial growth [30,31], and have demonstrated great potential as drug delivery systems [32,33]. SPI alone is unable to form nanofibers by electrospinning without the addition of a *co*-spinning polymer such as polyethylene oxide (PEO) [12,25,31,33,34], poly(vinyl alcohol) (PVA) [35,36] or other proteins such as silk fibroin [30]. Although, electrospinning of SPI-based nanofibers has been achieved, organic solvents such as HFIP[12], formic acid [30] or strong bases e.g. NaOH often in combination with heat [32,33,35,36] are most often used to overcome the solubility issues related to the inherent SPI protein composition and to facilitate the electrospinning process. Surfactants have also been added to lower the surface tension of water and support electrospinning of SPI [35,36]. While several studies have demonstrated promising applications of electrospun SPI-based nanofibers, the use of organic solvents, surfactants or strong bases can significantly compromise the biocompatibility, safety and sustainability of SPI-based nanofibers and limit their future use as safe and sustainable materials. Furthermore, encapsulation of a bioactive compound in the fibers can be challenging, as the bioactive compound must be stable under the conditions of material preparation e.g. in organic phases or under strong alkaline pH.

In this work, we employed an environmentally friendly method to fabricate sustainable and biocompatible electrospun nanofibers based on SPI with water being the only solvent, thus avoiding any use of organic solvents, strong bases or surfactants. PEO was used as a biocompatible *co*-spinning polymer to enhance intermolecular entanglement, and thus facilitate the electrospinning process. Sonication as a strategy to improve protein solubility, and hereby the formation of nanofibers by electrospinning was assessed by a thorough biophysical characterization of the electrospun samples. Furthermore, we produced nanofibers with a high SPI content and investigated the effect of the (w/w) content of SPI in the nanofibers on the morphology, brittleness and aqueous stability of the SPI/PEO nanofibers, which are key parameters for their future use. Finally, the biocompatibility and safety of the SPI/PEO nanofibers were demonstrated by exposure of human epithelial cell monolayers (TR146) to the nanofibers with the highest content of SPI. We propose that the presented strategies not only can provide innovative and sustainable solutions for improving electrospinning of SPI but also serve as a starting point for waterborne electrospinning of other proteins or protein isolates with the aim of producing greener and safer nanofiber-based materials.

2. Materials and methods

2.1. Materials

Vitablend Unisol DP IP Non GMO soy protein isolate (SPI, min. 90% protein) was kindly provided by Barentz ApS (Hoofddorp, The Netherlands). Polyethylene oxide (PEO, Mw 900 kDa), L-glutamine, penicillin, streptomycin, phenazine methosulfate (PMS), Dulbecco's modified Eagle's medium high-glucose (DMEM), Hanks' Balanced Salt solution (HBSS) and sodium dodecyl sulfate (SDS) were purchased from Sigma-Aldrich (St. Louis, MO, USA). 3-(4,5-dimethylthiazol-2-yl)-5-(3-carboxymethoxyphenyl)-2-(4-sulfophenyl)-2H-tetrazolium (MTS) was obtained from Promega (Madison, WI, USA). N-2-hydroxyethylpiperazine-N′-2-ethanesulfonic acid (HEPES) was obtained from PanReac AppliChem (Damstadt, Germany). Bicinchoninic acid (BCA) kit for protein determination and fetal bovine serum (FBS, HyClone) were obtained from Fisher Scientific (Roskilde, Denmark). The TR146 cell line was obtained from European Collection of Authenticated Cell Cultures (ECACC) (Public Health England, Porton, UK). Ultrapure water (18.2 MΩ·cm) was collected in-house by a PURELAB flex 4 system (ELGA, LabWater, High Wycombe, UK).

2.2. Fabrication of SPI/PEO nanofibers by electrospinning

A 12% (w/w) SPI suspension in ultrapure water, equal to 136 mg SPI per mL of ultrapure water, and a 4% (w/w) dispersion of PEO in ultrapure water, equal to 41.7 mg PEO per mL of ultrapure water, were prepared and stirred overnight at 4 °C (for SPI) or at room temperature (for PEO), respectively. SPI was sonicated on an ice bath on a S-4000-010 Misonix Sonicator (600 W, 220 *V*) (Bioventus LLC, Durham, NC, USA) for 30 min at an amplitude of 60% and pulse durations of on- and off-times of 10 s and 7 s, respectively. The sonicated SPI suspension and PEO dispersion were blended in 1:3, 1:2 and 1:1 (w/w) ratios (SPI suspension:PEO dispersion), leading to a theoretical content of SPI in the dry nanofibers of 50% (w/w), 60% (w/w) and 75% (w/w). SPI/PEO nanofibers with a theoretical content of 60% (w/w) SPI were also electrospun from a non-sonicated suspension of SPI. The blends were stirred for 30 min prior to electrospinning. The nanofibers were fabricated by electrospinning in an electrospinning hood (Linari Engineering S.R.L., Pisa, Italy) at a relative humidity of RH < 10%, a temperature of 23–26 °C, with a flow rate of 1 mL/h set on a syringe pump (Linari Engineering S.R.L., Pisa, Italy), a voltage supply in the range 15–17 kV (high-voltage generator (Linari Engineeering S.R.L., Pisa, Italy)) and a distance of 15 cm between the stainless steel plate collector (Linari Engineering S.R.L., Pisa, Italy) and the 20 G needle (Photo-Advantage, Ancaster, ON, Canada), which was fitted on a 5 mL syringe. SPI/PEO nanofibers with a theoretical content of 60% (w/w) SPI were also electrospun in absence of humidity control (RH > 35%).

2.3. Morphology assessment of electrospun SPI/PEO nanofibers by scanning electron microscopy (SEM)

Nanofibers were visualized under a Quanta™ 3D FEG scanning electron microscope (Thermo Fisher Scientific, Hillsboro, OR, USA) at an accelerated voltage of 2.00 kV. For imaging, samples were mounted

on carbon tapes on aluminum SEM stubs and sputter-coated with 6 nm gold under a Leica EM ACE200 gold coater (Leica Microsystems, Wetzlar, Germany). 200 individual nanofiber diameters were measured for each sample using the ImageJ software version 1.53 k (National Institute of Health, Bethesda, MD, USA).

2.4. Microscopic investigation of non-sonicated and sonicated SPI suspensions

12% (w/w) non-sonicated and sonicated SPI suspensions were prepared in ultrapure water, equal to 136 mg SPI per mL of ultrapure water, and diluted to final concentrations of SPI of 0.5 mg/mL. For the microscopic analysis of the samples, 250 μL of samples were placed on chambered slides and imaged at 1024 × 1024 pixels resolution under a Leica TCS SP5 confocal laser-scanning microscope set in transmission mode using a 40× objective (Leica Microsystems, Wetzlar, Germany).

2.5. Absorbance measurements

For the absorbance measurements, 12% (w/w) non-sonicated and sonicated SPI suspensions in ultrapure water, equal to 136 mg SPI per mL of ultrapure water, were prepared and diluted to a final concentration of SPI of 0.5 mg/mL. SPI/PEO nanofibers with a theoretical SPI content of 60% (w/w) were suspended in ultrapure water to a final concentration of SPI of 0.5 mg/mL. After preparation, all samples were stirred at 1000 rpm for 1 h prior to measurements. Absorption spectra were recorded by means of a JASCO *V*-760 spectrophotometer (JASCO Europe S.R.L., Cremella, Italy) at room temperature in the range 200–600 nm using a quartz cuvette with a 1 cm path length, a UV/Vis bandwidth of 2.0 nm, data intervals of 0.5 nm and a scan speed of 100 nm/min.

2.6. Rheology measurements

12% w/w SPI (sonicated or non-sonicated) and 4% w/w PEO suspensions, blended in different ratios, were analyzed by a steady state flow test on an AR-G2 rheometer (TA Instruments, Waters Corporation, Raleigh, NC) equipped with a cone of an angle of 1° and a diameter of 40 mm. The viscosity was determined at shear rates from 1 to 1000 s^{-1} at 25 °C with a 5 min equilibration period prior to each measurement. The tolerance was set to 5% with a maximum measuring time of 1 min for each shear rate.

2.7. Assessment of changes in secondary structure by circular dichroism (CD)

Samples (non-sonicated or sonicated SPI suspensions and SPI/PEO nanofibers) were prepared as described in Section 2.5. CD measurements were acquired in the far-UV region (190–260 nm) on a JASCO J-715 spectropolarimeter, equipped with a JASCO PCT 348 WI temperature control system (JASCO Europe S.R.L., Cremella, Italy), set to 25 °C. A quartz cuvette with a 0.5 mm path length was used, and spectra were collected with a scan speed of 50 nm/min, 1 nm bandwidth and a data pitch of 0.1 nm. Four scans were recorded and averaged for each sample. The CD data were smoothed by a 4-point Savitzky-Golay algorithm.

2.8. Assessment of changes in tertiary structure by fluorescence spectroscopy

Fluorescence spectroscopy measurements were acquired for samples (non-sonicated, sonicated SPI suspensions and SPI/PEO nanofibers) prepared as described in Section 2.5 using a JASCO-FP-8500 spectrofluorometer equipped with a JASCO ETC-815 Peltier temperature control system (JASCO Europe S.R.L., Cremella, Italy) set to 25 °C. Emission spectra were acquired in the wavelength range 275–550 nm, using a quartz cuvette with a 1 cm path length, an excitation wavelength λ_{exc} = 280 nm, an excitation bandwidth of 5 nm, an emission bandwidth of 2.5 nm, a response time of 1 s, data intervals of 0.5 nm and a scan speed of 100 nm/min.

2.9. Secondary structure analysis by Fourier transform infrared (FTIR) spectroscopy

For FTIR analysis, measurements were acquired for non-sonicated and sonicated SPI suspensions prepared in D_2O and SPI/PEO nanofibers with a theoretical SPI content of 60% (w/w) suspended in D_2O to a final concentration of SPI of 20 mg/mL. Measurements were performed using a Bruker Vertex 70 spectrometer equipped with a doped triglycine sulfate (DTGS) detector under continuous purging of N_2 dry atmosphere. Approximately 20 μL of sample were loaded into a cell equipped with CaF_2 windows with a spacer with a thickness of 50 μm. Absorption measurements were performed in the frequency range 400–7000 cm^{-1} and 64 scans were recorded for each measurement with a resolution of 2 cm^{-1}. The spectrum of the empty cell was used as a reference for the absorption spectrum, and the OPUS software was used to clean the spectra from absorption bands from water vapor. The D_2O spectrum was subtracted from all spectra. Fitting of the amide I band was performed in terms of five Gaussian components using the Origin 2020.Ink software. The following equation (Eq.(1)) was used:

$$I(\nu) = \sum_{i=1}^{n} A_i e^{\left[-\frac{(\nu-\nu_i)^2}{2\sigma_i^2}\right]} \quad (1)$$

where I is the infrared intensity and ν_i, σ_i and $A_i = {}^{1}/_{\sigma_i\sqrt{2\pi}}$ are the peak frequency, width and area of the i^{th} component, respectively. For the fitting procedure, the peak frequency of the selected five components [37,38] was kept fixed at 1620 cm^{-1}, 1635 cm^{-1}, 1653 cm^{-1}, 1665 cm^{-1} and 1680 cm^{-1} and the spectral width was shared. The fractional area, indicating the relative amount of secondary protein structure in each spectrum, was defined by the following equation (Eq. (2)):

$$A_i\,(\%) = \frac{A_i}{\sum_{i=1}^{n} A_i}\% \quad (2)$$

2.10. Assessment of composition of nanofibers by attenuated total reflectance FTIR (ATR-FTIR) spectroscopy

ATR analysis on powders of SPI and PEO and on dry SPI/PEO nanofibers with a theoretical SPI content of 60% (w/w) was conducted using a Bruker ALPHA FTIR spectrometer equipped with a platinum ATR device (Bruker Optics, Ettlingen, Germany). Spectra were recorded in the wavelength range 4000–400 cm^{-1} as an average of 24 scans and with a spectral resolution of 4 cm^{-1}. Background contribution was subtracted from all spectra.

2.11. Determination of the elongation at break of SPI/PEO nanofibers by dynamic mechanical analysis

Nanofiber mats were cut into rectangular shapes (6.4 mm × 30.0 mm). The samples were mounted using film tension clamps and analyzed on a dynamic mechanical analyzer (Q800, New Castle, DE, USA).A preload force of 0.01 N and initial displacement of 0.2% were set before the analysis. The samples were subjected to a displacement ramp of 500 μm/min. The obtained stress-strain curves were analyzed in Thermal Advantage Software v 5.5.2 (TA Instruments, New Castle, DE, USA) to determine the elongation at break, at the strain at which the material could not stretch further. The results were compared by an unpaired student two-tailed *t*-test. An F-test was conducted to compare variances. Welch's correction was applied in case of significantly ($p < 0.05$) different variances.

2.12. Disintegration of electrospun SPI/PEO nanofibers in water and release of SPI

For assessment of the disintegration and release of SPI, 10 mm discs of nanofibers were immersed in 1.5 mL of ultrapure water in the wells of a 24-well plate (Sigma-Aldrich, St. Louis, MO, USA) on a shaking table (100 rpm) at room temperature. Samples of 100 μL were withdrawn from the wells at different time points (1, 15, 30, 60, 120, 180, 240, 300 and 360 min) and transferred to LoBind Eppendorf® tubes (Sigma-Aldrich, St. Louis, MO, USA) and frozen at −20 °C. At each time point, 100 μL of ultrapure water was added to the wells to keep the release volume constant. To visualize the degree of disintegration, samples were further imaged over time, in absence of shaking. The withdrawn samples were analyzed by the bicichoninic acid (BCA) assay for protein determination by the microplate procedure. Briefly, the samples were thawed and 25 μL were transferred to a transparent 96-well plate and incubated at 37 °C with 200 μL of BCA working reagent with mild agitation (50 rpm) for 30 min. The absorbance of the samples was then measured at 562 nm in a plate reader (POLARstar OPTIMA, BMG LABTECH, Ortenberg, Germany). The method was *v*alidated using SPI standards in ultrapure water and SPI concentrations ranged from 20 to 1280 μg/mL ($R^2 \geq 0.99$).

2.13. Biocompatibility assessment of SPI/PEO nanofibers by an in vitro cell based assay

TR146 cells (human squamous cell carcinoma, buccal) were cultured in Corning Costar polystyrene culture flasks (175 cm^2, Sigma-Aldrich, St. Louis, MO, USA) in DMEM supplemented with L-glutamine (2 mM), penicillin (100 U/mL), streptomycin (100 μg/mL), and FBS (10% (v/v)) in a humidified incubator at 37 °C with 5% CO_2. 125,000 TR146 cells/well were seeded in flat-bottom, transparent 12-well plates (Sigma-Aldrich, St. Louis, MO, USA) and cultured for two days under the aforementioned conditions. The cells were washed twice in 2 mL of warm (37 °C) 10 mM HEPES in HBSS pH 6.8 (hHBSS) prior to exposure to 1.5 mL sonicated SPI suspension (1.5 mg/mL), PEO (0.5 mg/mL) or to round discs of 10 mm in diameter of SPI/PEO nanofibers with a theoretical SPI content of 75% (w/w) placed in 1.5 mL hHBSS. The cells were incubated for 3 h at 37 °C. After treatment, the nanofibers were removed (to the extent possible) and the cells were washed twice in hHBSS pH 6.8. The viability of the cells after exposure was evaluated by the MTS/PMS colorimetric assay by incubating the cells at 37 °C for 120 min with 1 mL reagent solution containing 240 μg/mL MTS and 2.4 mg/mL PMS in hHBSS buffer with mild shaking (50 rpm). Hereafter, 100 μL in quadruplicates of the metabolized MTS/PMS solution from each well was transferred to a transparent 96-well plate, and the absorbance was measured at a wavelength of 492 nm in a plate reader (POLARstar OPTIMA, BMG LABTECH, Ortenberg, Germany). The absorbance at 690 nm was subtracted from the primary absorbance measurements at 492 nm. Cells were treated in triplicates for nanofibers prepared on two different days. Cell passages 5, 6 and 7 were used. The absorbance of the cells treated with 0.2% SDS was defined as the negative control (Abs_{neg}, 0% cell viability) and positive control was defined as cells incubated with hHBSS (Abs_{pos}, 100% cell viability) and the relative cell viability as compared to control was determined by the following equation (Eq. (3)):

$$\text{Relative cell viability } (\%) = \frac{Abs_{sample} - Abs_{neg}}{Abs_{pos} - Abs_{neg}} \times 100\% \quad (3)$$

3. Results and discussion

3.1. Solution and ambient conditions affect morphology of electrospun SPI-based nanofibers

It is well known that solution properties, electrical field and ambient conditions must be optimized to achieve continuous electrospinning of smooth nanofibers without artifacts such as beading [22]. Proteins such as SPI are particularly challenging to electrospin in water as low solubility and restricted entanglement between proteins in bulk results in incomplete fiber formation by electrospinning. Here, PEO was therefore added to SPI as a *co*-spinning polymer; a well-known strategy to improve solution viscosity and to facilitate electrospinning of molecules that display limited intermolecular entanglement. Electrospinning from aqueous-based solutions is thus favored, avoiding organic solvents, strong bases or surfactants to minimize the environmental impact and improve human safety of the electrospun SPI-based nanofibers. The specific aim was therefore to evaluate strategies to improve waterborne electrospinning of SPI.

SPI was not spinnable in the absence of PEO. Mats of nanofibers electrospun from (non-sonicated) SPI with PEO were inhomogeneous, the nanofibers contained large particles/aggregates of potentially undissolved material as visualized by SEM (Fig. 1A) and the spinning process was neither continuous nor robust. Sonication of SPI in water prior to mixing with PEO was attempted to improve the aqueous solubility of the protein isolate. Sonication of the protein isolate may also induce conformational changes. These will lead to the exposure of areas of the proteins, allowing new intermolecular interactions and eventually improving the entanglement between the molecules. Electrospinning of sonicated SPI with PEO at high humidity was continuous and resulted in a homogeneous network of beaded nanofibers (Fig. 1B). The size, shape and distribution of the beads along the nanofibers (Fig. 1B) were significantly more uniform as compared to the particles of undissolved material seen on the nanofibers electrospun from non-sonicated SPI (Fig. 1A). This indicates that the formation of the small beads similar in size (Fig. 1B) was most likely due to an instability in the electrospinning process. Delayed solidification of nanofibers during electrospinning because of slow solvent evaporation can cause beaded nanofibers, as reported by others [39,40]. The high boiling point of water is a significant challenge in electrospinning from aqueous solutions; and to improve the quality of the nanofibers and prevent bead formation, electrospinning of SPI/PEO was conducted under conditions of low humidity to enhance evaporation of water by other means than the addition of volatile organic solvents. Nanofibers made from sonicated SPI electrospun under low humidity were homogeneous, smooth and without artifacts such as beading (Fig. 1C). This result indeed highlights the importance of the combined optimization of solution properties and ambient conditions for effective electrospinning of proteins or protein isolates such as SPI. Noteworthy, the combined effect of SPI sonication and electrospinning of SPI/PEO under low humidity was hereby demonstrated to be a simpler, greener and safer method to produce SPI-based nanofibers as compared to the traditional methods that involve organic solvents, strong bases and surfactants. We propose that the presented strategies not only can improve the electrospinning of SPI in water, but also facilitate waterborne electrospinning of other types of proteins or protein isolates, as the challenges of electrospinning of SPI, e.g. low solubility in water and low intermolecular entanglement, are general for many proteins.

3.2. Improved electrospinnability of sonicated SPI is due to changes in the properties of the SPI suspension

SPI forms a turbid suspension in water, and the protein isolate is only partially dissolved as visible precipitation/phase separation of SPI was observed within 45 min in the absence of sonication (Fig. 2A, top). Sonication of SPI in water induced visible changes in the suspension (Fig. 2A). The sonicated suspension of SPI was turbid, but no precipitation of SPI was visible within several hours; thus sonication significantly improves the stability of the suspension (Fig. 2A). In accordance, large structures in the non-sonicated SPI suspension were fragmented into less abundant and smaller structures by sonication as visualized under the microscope (Fig. 2A, bottom).

Fig. 2B shows the representative absorption spectra in the spectral

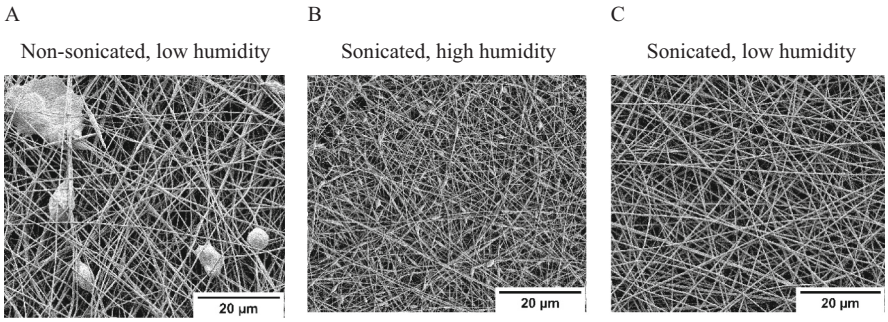

Fig. 1. Strategies (solution sonication and electrospinning at low humidity) to improve electrospinning of SPI/PEO nanofibers. Representative SEM images of electrospun A) non-sonicated SPI (60% (w/w)) with PEO at low humidity, B) sonicated SPI (60% (w/w)) with PEO at high humidity (>35% RH) and C) sonicated SPI (60% (w/w)) with PEO at low humidity (<10% RH). $N = 2$, where N represents the number of nanofiber mats prepared on separate days.

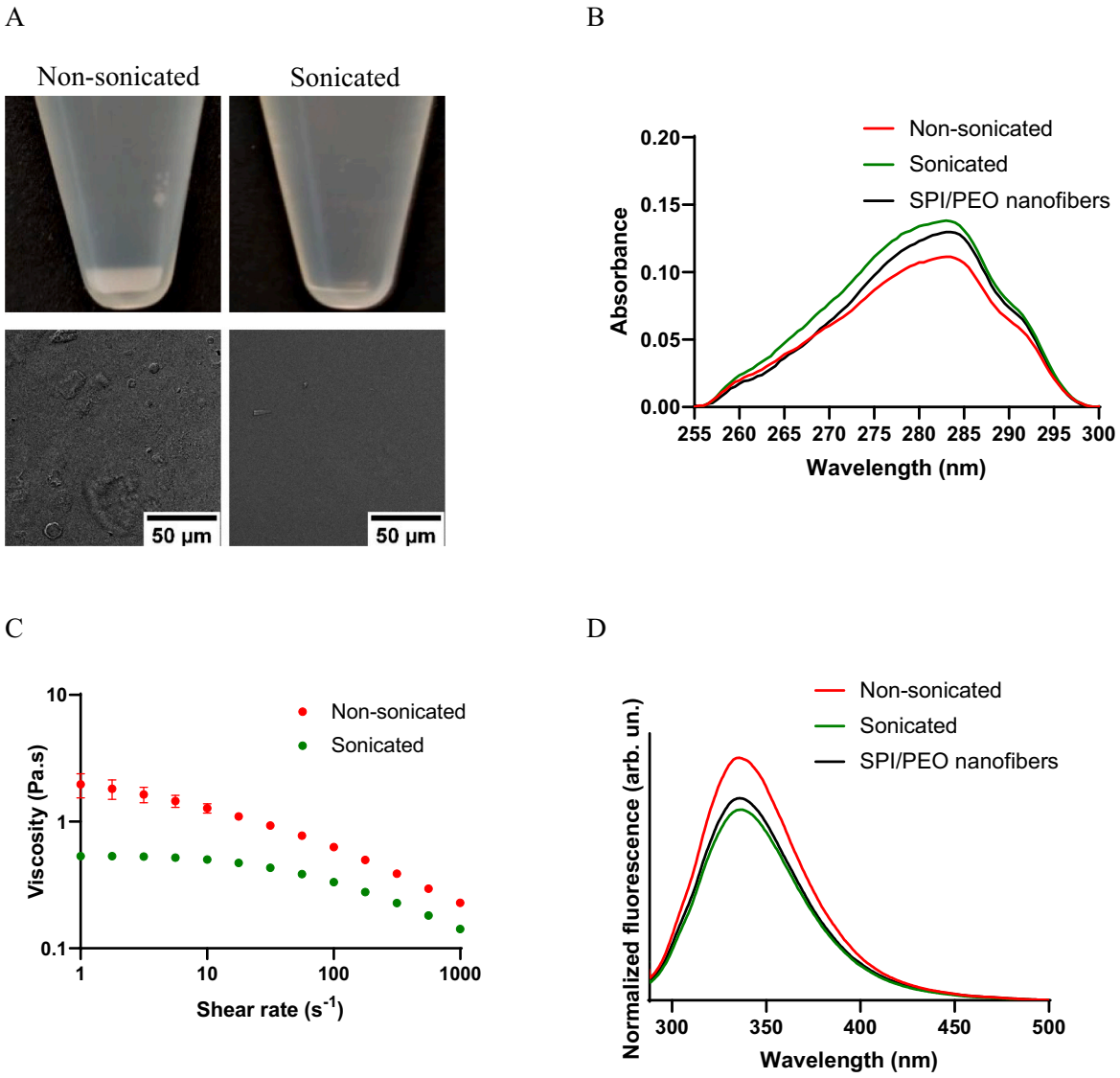

Fig. 2. Sonication induces fragmentation of large structures into smaller and improves solubility of SPI. A) Image of non-sonicated and sonicated SPI in water (diluted to 0.5 mg/mL). Precipitation was visible after ≥45 min for the non-sonicated SPI suspension (top). Larger structures in the non-sonicated suspension fragment into smaller structures in the sonicated suspension as visualized under the microscope (bottom). B) Representative UV–Vis absorbance curves for non-sonicated SPI, sonicated SPI and SPI/PEO nanofibers (sonicated, 60% (w/w) SPI) suspended in water, resulting after removal of turbidity contribution (Supplementary data, Fig. S1). $N = 3$, $n = 1$–2. C) Rheological profiles of non-sonicated and sonicated SPI/PEO suspensions presented as mean ± standard deviation. Error bars are not shown for standard deviations smaller than the round symbols. $N = 2$, $n = 2$. D) Representative curves of intrinsic fluorescence intensity signal for non-sonicated SPI, sonicated SPI and SPI/PEO nanofibers (sonicated, 60% (w/w) SPI) suspended in water. Data normalized by absorbance of samples at the excitation wavelength. N = 2, n = 2. For all, N represents the number of samples prepared on different days, and n the number of measurements per sample.

region characteristic of the aromatic residues after suitable subtraction of a baseline to remove turbidity contribution (Supplementary data, Fig. S1). A structured peak centered at about 280 nm is observed for suspensions of non-sonicated SPI, sonicated SPI and an aqueous suspension resulting from disintegrating the SPI/PEO nanofibers (sonicated, 60% (w/w) SPI) in water. All spectra are characterized by a high contribution of turbidity, this indicating the presence of undissolved structures in suspension and thus limited solubilization of SPI. As expected, this is more evident in the non-sonicated suspension (Supplementary data, Fig. S1). The aim of these measurements is to qualitatively compare the protein concentration in the characterized samples. The low solubility of SPI in water is related to the high content of hydrophobic amino acids in the protein isolate, which unfortunately also limits the usage of SPI for biomedical applications [41]. In accordance with the visual examination of the samples (Fig. 2A), the higher absorbance recorded for sonicated SPI (prepared at the same nominal concentration), as compared to the non-sonicated SPI indicates an improvement in the protein solubility of SPI via sonication (Fig. 2B). This can be directly related to the improved electrospinnability of the sonicated SPI suspension, where increased solubility of SPI results in increased stability of the electrospinning process. General approaches to modify SPI protein structure and improve its solubility include amongst others pH shifting (alkaline or acidic), heat treatment and sonication [42–44]. Importantly, in the present work, the solubility of SPI was increased only via simple sonication without alkaline or heat treatment. Furthermore, it should be noted that, as expected, the absorbance of SPI/PEO nanofibers (sonicated, 60% (*w*/w) SPI) suspended in water was similar to the recorded absorbance of sonicated SPI at the same nominal concentration.

Significant changes in flow properties of the SPI suspension due to sonication were also evident from changes in the rheological profile before and after sonication of SPI. Non-sonicated and sonicated SPI displayed significantly different rheological profiles (Fig. 2C). The presence of insoluble material in the suspension of non-sonicated SPI increased the viscosity as compared to the sonicated SPI (Fig. 2C). Both sonicated and non-sonicated SPI mixed with PEO displayed clear shear thinning behavior due to the presence of a significant amount of PEO i.e. a decrease in viscosity with increase in shear rate. Only the rheological profile for sonicated SPI mixed with PEO showed a clear 1st Newtonian plateau (shear rate 1–10 s^{-1}) in the evaluated range of shear rates (1–1000 s^{-1}) (Fig. 2C). O'Flynn et al.[41] reported a significant increase of viscosity of SPI at pH 6.9 due to heating (90 °C, 20 min) leading to additional denaturation/aggregation of the two major protein fractions of SPI i.e. β-conglycinin and glycinin. In contrast, a decrease in viscosity after sonication of SPI could indicate improved solubility and/or fragmentation of the insoluble forms of protein fractions in the SPI suspension (Fig. 2C).

To gain deeper information on the effect of sonication on the SPI suspension, fluorescence spectroscopy was used for its exquisite sensitivity to environmental properties in the surroundings of intrinsic chromophores commonly present in protein structures [45]. The intrinsic emission of SPI is attributed to aromatic residues in the protein structure and in particular to tryptophans [46]. Variations in the fluorescence spectral shape and intensity are generally attributed to variations in the environment of these chromophores as they are particularly sensitive to their environment polarity. A decrease of SPI fluorescence intensity can be attributed to the exposure of tryptophan residues to the solvent [46]. Non-sonicated SPI suspension displays a higher intrinsic fluorescence intensity signal as compared to sonicated SPI and SPI/PEO nanofibers (sonicated, 60% (*w*/w) SPI) suspended in water (Fig. 2D). This may suggest a larger hydrophobicity or rigidity in the environment of tryptophan residues present in the protein structures. This may furthermore indicate a more tightly packed supramolecular organization ofthe protein aggregates present in the suspension of non-sonicated SPI. Fragmentation of the larger structures of the non-sonicated SPI suspension into smaller ones by sonication, may result in increased solvent accessibility of the tryptophan residues that are buried in the internal part of the structures (of the non-sonicated SPI suspension).

Sonication did not affect the protein secondary structure of SPI as shown by the normalized CD spectra of sonicated and non-sonicated SPI and SPI/PEO nanofibers (sonicated, 60% (w/w) SPI) suspended in water (Fig. 3A*)*. Importantly, the secondary structure of the protein constituents of SPI was also not affected by electrospinning the sonicated suspension of SPI into nanofibers (Fig. 3A). The CD spectra display a negative peak between 200 and 240 nm, which is indicative of a high β-sheet content as previously reported for SPI [42,47,48]. Fig. 3B represents a broad absorption band of SPI in the amide I region, centered at around 1640 cm^{-1} [37,38,49]. The observed spectral shape is broadened towards lower wavenumbers (Fig. 3B), in the region 1628–1614 cm^{-1}, where contribution of aggregated β-sheet structure stabilized by H-bonds is found [38,50]. Indeed, deconvolution of the amide I band by fitting of the Gaussian function highlighted further the high β-sheet content of SPI, both inter- and intramolecular (1620 cm^{-1}, aggregated 16%; 1635 cm^{-1}, native 36%; 1680 cm^{-1}, aggregated 7%) (Fig. 3C). The presence of α-helical secondary structure (1653 cm^{-1}, native, 28%) and turns and loops (1665 cm^{-1}, native 13%) was also detected, although in lower percentages (Fig. 3C).

Overall, the in-depth biophysical characterization and rheological profiling of SPI before and after sonication indicate that large structures in the SPI suspension fragment into smaller structures during sonication, and SPI solubility improves, which make the SPI suspension more suitable for electrospinning. Interestingly, SPI/PEO nanofibers (sonicated, 60% (w/w) SPI) present the same profile in the conducted analyses as the sonicated SPI suspension that they originate from, thus confirming that electrospinning does not significantly modify the molecular structure of SPI.

ATR-FTIR spectra of SPI and PEO powders and SPI/PEO nanofibers (sonicated, 60% (w/w) SPI) are reported in Fig. 4. The characteristic amide I protein region (1700–1600 cm^{-1}) assigned to stretching vibrations of the C═O of the protein backbone related to β-sheet protein conformation is present both in the ATR spectrum of SPI and SPI/PEO nanofibers (sonicated, 60% (w/w) SPI) [48]. The characteristic protein amide II absorption band (1600–1500 cm^{-1}) is also present in the spectrum of SPI and SPI/PEO nanofibers (sonicated, 60% (w/w) SPI) and can be attributed to C—N and N—H stretching vibrations. The peak of SPI at 3280 cm^{-1} could be attributed to -OH and N—H stretching vibration and formation of hydrogen bonds in the SPI/PEO nanofibers [51] or to H-O-H stretching that have previously been observed in protein-containing samples [52]. The characteristic peaks of C-O-C and CH_2 stretching vibrations at 1100 cm^{-1} and 2900 cm^{-1}, respectively, are both present in the PEO spectrum [13,53]. The detection of the characteristic SPI and PEO peaks in the spectrum of SPI/PEO nanofibers confirms the presence of both SPI and PEO in the nanofibers after spinning (Fig. 4).

3.3. SPI to PEO ratio affects the mechanical properties of nanofiber mats

Materials made from protein often display poor mechanical properties i.e. the materials are brittle, inflexible and break easily under stress [54]. In general, poor mechanical properties is a significant limitation for the development of protein-based materials for example for the material to be able to bend to the curved surfaces of the body as bandages for wound healing or patches for drug delivery [6]. Good mechanical properties are also requirements of textiles, filters for water and air, and for materials used for food packaging. The effect of the protein content on the morphological properties and the elongation at break of SPI/PEO nanofibers was therefore investigated. Nanofibers with a SPI (sonicated) content up to 75% (w/w) was achieved by electrospinning under the aforementioned conditions. In comparison, Cho et al. [35] reported the maximum content of SPI in nanofibers electrospun with PVA in the presence of NaOH to be ≤50% (w/w) to avoid beaded fibers, and Thirugnanaselvam et al.[31] reported a maximum content of 40% SPI

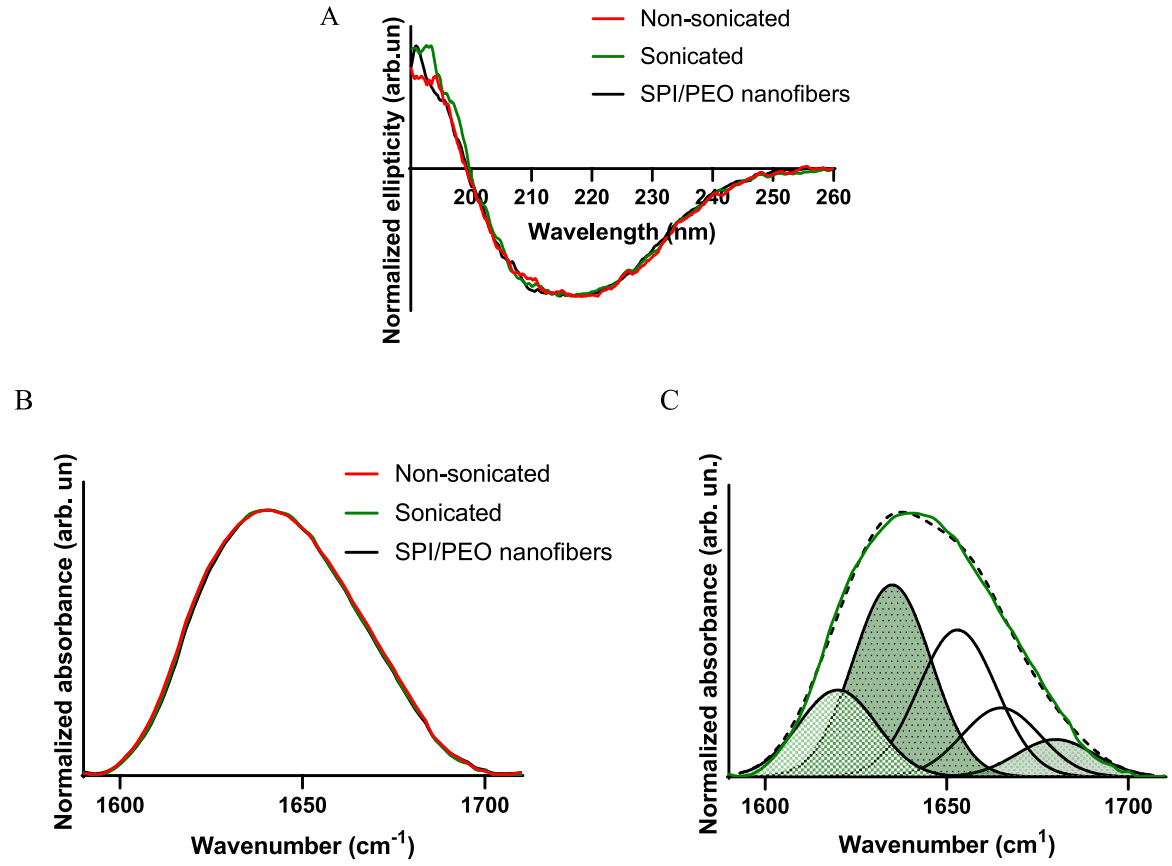

Fig. 3. Sonication does not affect the secondary structure of SPI. A) Representative circular dichroism curves of for non-sonicated SPI, sonicated SPI and SPI/PEO nanofibers (sonicated, 60% (w/w) SPI) suspended in water. Data normalized by maximum negative ellipticity signal and smoothed by a 4-point Savitzky-Golay algorithm. $N = 2$, $n = 2$. B) Representative peaks of FTIR spectra for non-sonicated SPI, sonicated SPI and SPI/PEO nanofibers (sonicated, 60% (w/w) SPI) suspended in D_2O, at the amide I region. Data normalized by maximum absorbance. N = 2, n = 2. For all, N represents the number of samples prepared on different days, and n the number of measurements per sample. C) Representative spectral deconvolution in Gaussian components of FTIR spectrum with spectral components centered at 1620 cm^{-1}, 1635 cm^{-1}, 1653 cm^{-1}, 1665 cm^{-1} and 1680 cm^{-1}. Each component is assigned to a certain backbone conformation and fractions of the total area of the amide I band for each of the components used for the deconvolution are shown.

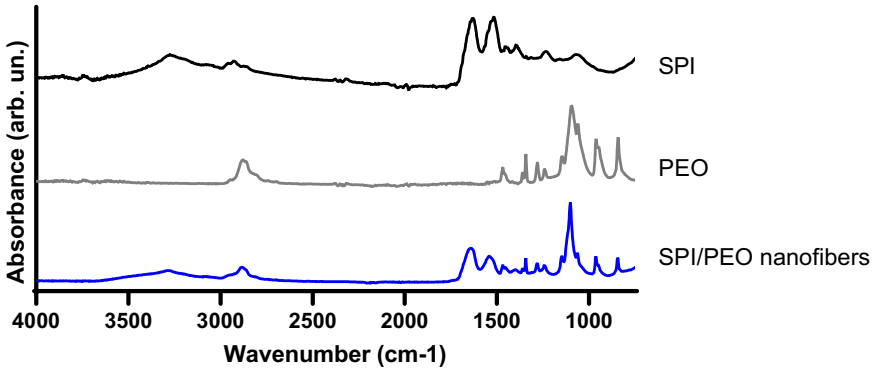

Fig. 4. Composition analysis of electrospun SPI/PEO nanofibers by ATR-FTIR. Representative ATR-FTIR curves (normalized) of SPI powder, PEO powder and SPI/PEO nanofibers (sonicated, 60% (w/w) SPI). $N = 2$, $n = 2$, where N represents the number of samples analyzed on different days and n the number of measurements per sample. Two batches of SPI/PEO nanofibers were analyzed.

(w/w) in nanofibers electrospun with PEO in the presence of NaOH, as a content of 60% SPI (w/w) could not be reached. Thus, a significantly higher SPI content in the nanofibers was achieved by the presented method. Increasing the ratio of SPI to PEO significantly above 75% (w/w) under the presented conditions was expected to result in an unstable electrospinning jet, and electrospinning of nanofibers of higher SPI content was therefore not attempted. In general, the nanofibers were homogeneous, smooth and without artifacts such as beadings as visualized by SEM (Fig. 5A). Although, sonication did not facilitate complete dissolution of SPI, it is interesting to note that electrospinning of a turbid (protein) suspension with PEO resulted in the formation of smooth fibers in the nm size range. Nanofibers of the lowest SPI content of 50% (w/w) were thinner than nanofibers of the highest SPI content i.e. 60% and 75% (w/w) (Fig. 5B). SEM analysis revealed a few breakages in

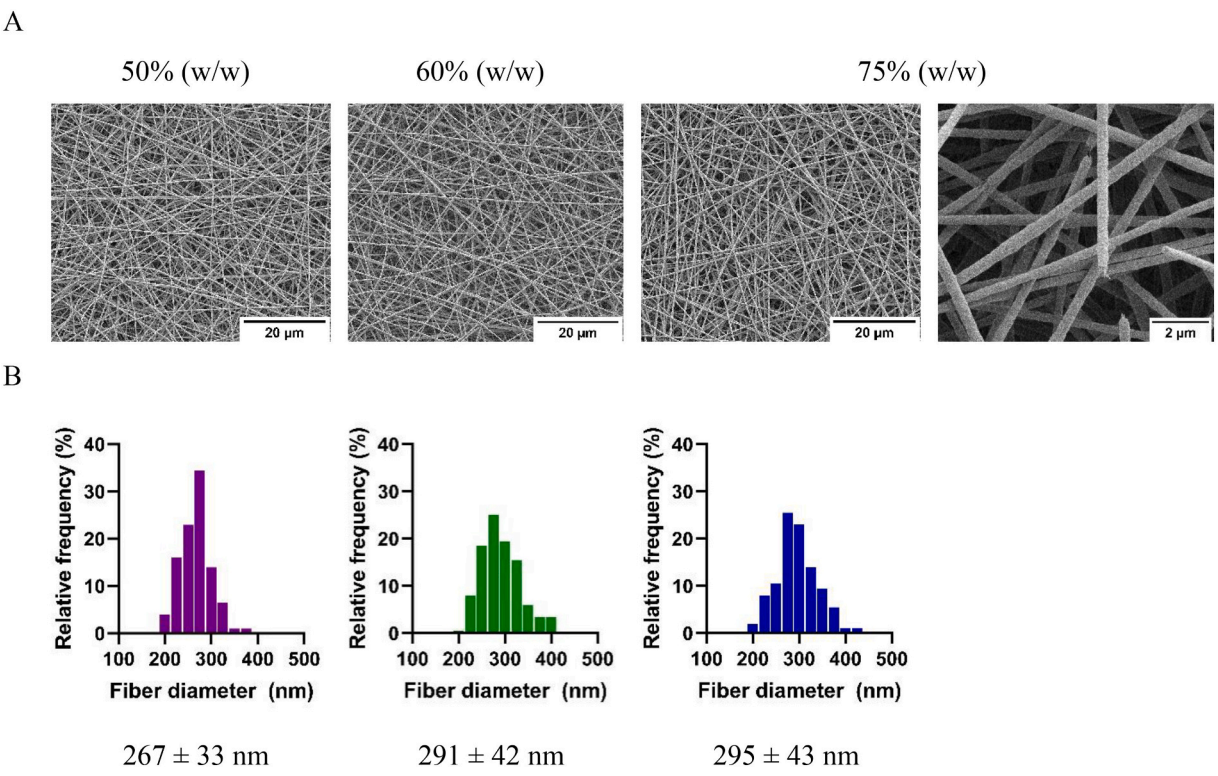

Fig. 5. The soy to PEO ratio affect the morphological appearance of electrospun nanofibers. A) Representative SEM images of electrospun SPI/PEO nanofibers with a SPI content of 50% (w/w), 60% (w/w) or 75% (w/w). $N = 2$. B) Size distribution of electrospun SPI/PEO nanofibers with a SPI content of 50% (w/w), 60% (w/w) or 75% (w/w). Mean diameter ± standard deviation is given. N = 2, $n = 200$, where N represents the number of batches of nanofibers and n the number of measurements per sample.

individual nanofibers with 75% (w/w) SPI (Fig. 5A), which were not evident in samples of lower SPI content. This could indicate that the nanofibers of the highest SPI content would be the more brittle.

Thus, dynamic mechanical analysis (DMA) was conducted to evaluate the elongation at break (EAB) of the SPI/PEO nanofiber mats depending on the content of SPI. SPI/PEO nanofiber mats of various SPI content were stretched until their breaking point, and the elongation at break i.e. the maximum strain (%) reached before breakage was determined. In accordance with the morphological assessment of the nanofibers (Fig. 5A), mats of SPI/PEO nanofibers with the highest content of SPI i.e. 75% (w/w) could stretch <20% of their initial length and the sample was thus statistically significantly ($p < 0.05$) more brittle than nanofiber mats with a lower SPI to PEO ratio (Fig. 6A). Nevertheless, the ability of these nanofiber mats, i.e. SPI/PEO nanofiber mats with 75% (w/w) SPI content, to stretch at this level could be attributed to the β-sheet content of SPI, which is indicative of materials with robust mechanical properties [48]. As expected, the elongation at break of the SPI/PEO nanofiber mats increased with the content of the plasticizer PEO in the fibers. Interestingly, a small relative decrease in SPI content (10–15% (w/w)) in the nanofibers resulted in a statistically significant ($p < 0.05$) improvement of the mechanical properties of the nanofiber mats (Fig. 6A).

The effect of PEO was also directly seen in the rheological profile of the SPI/PEO suspensions that were electrospun (Fig. 6B). All suspension were non-Newtonian and displayed shear-thinning properties (Fig. 6B). Increasing the content of SPI, and thus decreasing the content of PEO, resulted in a significant decrease in the viscosity of the SPI/PEO suspensions (Fig. 6B). Thus, the addition of PEO increased the viscosity of

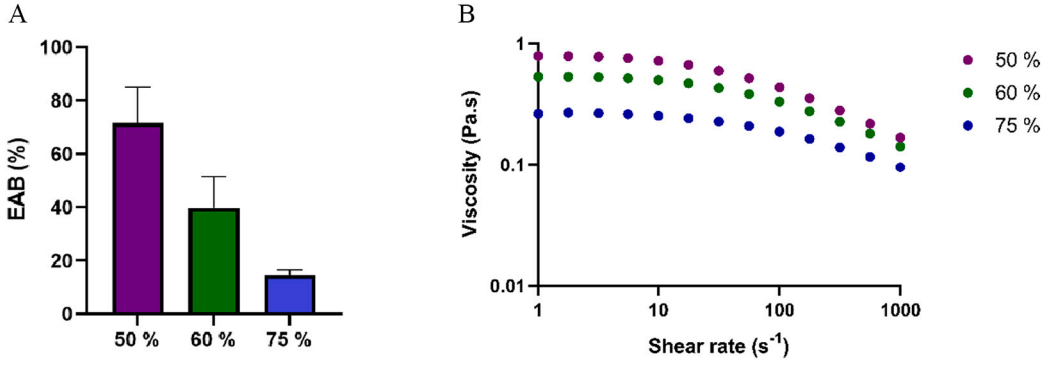

Fig. 6. The brittleness of SPI/PEO nanofiber mats depends on the SPI to PEO ratio. A) Elongation at break (EAB) of SPI/PEO nanofiber mats with a SPI content of 50% (w/w), 60% (w/w) or 75% (w/w). $N = 2$, $n = 3$, where N represents the number of batches of nanofibers prepared and n the number of measurements per batch. Results are presented as mean + standard deviation. B) Results presented as mean + standard deviation. B) Rheological profile of SPI/PEO suspensions of sonicated SPI in different PEO to SPI ratios i.e. 50%, 60% or 75% SPI (w/w). Results presented as mean. The standard deviations are smaller than the round symbols and are therefore not shown. N = 2, $n = 2$, where N represents the number of samples prepared on different days and n the number of measurements per sample.

the SPI suspensions to be electrospun. An increase in viscosity is an indicator of improved intermolecular entanglement within the molecules in bulk, here PEO and SPI. Nevertheless, electrospinning of the tested SPI to PEO ratios resulted in the formation of smooth nanofibers in the recorded viscosity range suggesting that a sufficient degree of intermolecular entanglement was obtained.

3.4. Disintegration of SPI-based nanofibers depends on initial protein content

In general, some applications require the material to be, to a certain extent, resistant and morphologically stable in aqueous-based environments e.g. for water filtration purposes, as wound dressings in a moist wound bed or for drug delivery applications for sustained release. PEO is highly water-soluble, and nanofibers made solely from PEO dissolve immediately when brought in contact with water. In contrast, SPI forms a turbid suspension when hydrated (Fig. 2A). The aqueous stability and the degree of disintegration of electrospun SPI/PEO nanofibers of various protein content were assessed. Round discs of nanofibers with the lowest content of SPI (50% (w/w)) and the highest content of PEO lost their round shape within minutes and disintegrated almost completely within 24 h in water (Fig. 7A). In contrast, round patches of nanofibers with the highest content of SPI (sonicated, 75% (w/w)) maintained their round shape for at least 24 h (Fig. 7A). The amount of protein released from the nanofibers in water over time was quantified. In accordance with the visual appearance of the disintegration of the nanofiber discs (Fig. 7A), nanofibers that displayed the highest degree of disintegration i.e. nanofibers with 50% (w/w) SPI also showed the highest relative release of protein compared to nanofibers of lower SPI content (Fig. 7B).

Low stability of a material in aqueous medium is a significant challenge for many biomedical applications of e.g. films, hydrogels and electrospun nanofibers; protein-based materials are no exception. Cross-linking is often employed to improve the morphological stability of protein-based materials in water. Chemical agents such as small chain aldehydes e.g. glutaraldehyde (GTA) have been widely used for cross-linking of proteins to improve the aqueous stability of protein-based materials [55,56]. However, chemical cross-linking agents such as GTA raise serious concerns for their potential negative impact on human health [57,58]. It is therefore an intriguing property that SPI-based nanofibers discs of high protein-content to a great extent maintain their shape for at least 24 h after being submerged in water without the need for cross-linking.

3.5. Waterborne electrospinning of SPI/PEO for biocompatible and sustainable nanofibers

Organic solvents not only compromise the biocompatibility of the nanofibers but also lead to release of hazardous solvents to the surroundings during electrospinning, which is not in line with green manufacturing procedures [24]. To demonstrate the biocompatibility of waterborne SPI/PEO based nanofibers, human epithelial cell monolayers (TR146 cells) were exposed to SPI/PEO nanofibers (sonicated, 75% (w/w) SPI), SPI and PEO for 3 h, and the relative cell viability compared to cells exposed to control (isotonic buffer) was assessed. No effect on the relative cell viability was found for the SPI/PEO nanofibers, nor for their individual components i.e. neat SPI or PEO (Fig. 8). The results are indeed not surprising as both SPI (Section in Code of Federal Regulations (CFR)/CAS Reg. No. 977076–84-8) are classified as Generally Regarded As Safe (GRAS) and PEO has been approved as an 'Inactive Ingredient' (Unique Ingredient Identifier number 16P9295IIL) by the US Food and Drug Administration (FDA), and the nanofibers were electrospun in water as the only solvent. Biocompatibility is an indispensable property for clinical translation of nanofibers into materials for e.g. drug delivery, tissue engineering or wound healing purposes. Furthermore, many other potential applications proposed for protein-based materials such as textiles, filters for air- and water-filtration or as alternatives to plastic for food packaging could also have a direct impact on human health. Indeed, waterborne electrospinning is believed to be a very important milestone towards the environmentally friendly

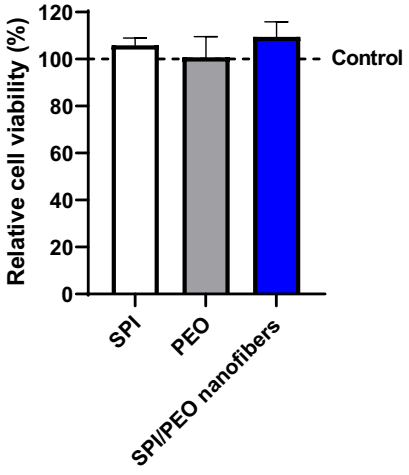

Fig. 8. Exposure of human epithelial cell monolayers (TR146 cells) to SPI/PEO nanofibers demonstrated good biocompatibility of the nanofibers. Relative cell viability compared to Control (10 mM HEPES in HBSS pH 6.8, 100% cell viability) of human epithelial cell monolayers (TR146 cells) exposed for 3 h to sonicated SPI (1.5 mg/mL), PEO (0.5 mg/mL) and 10 mm discs of SPI/PEO nanofibers (75% (w/w) SPI content). $N = 2$, $n = 3$, where N represents the number of cell passages and batches of nanofibers, and n represents the number of samples evaluated per batch. Results presented as mean + standard deviation.

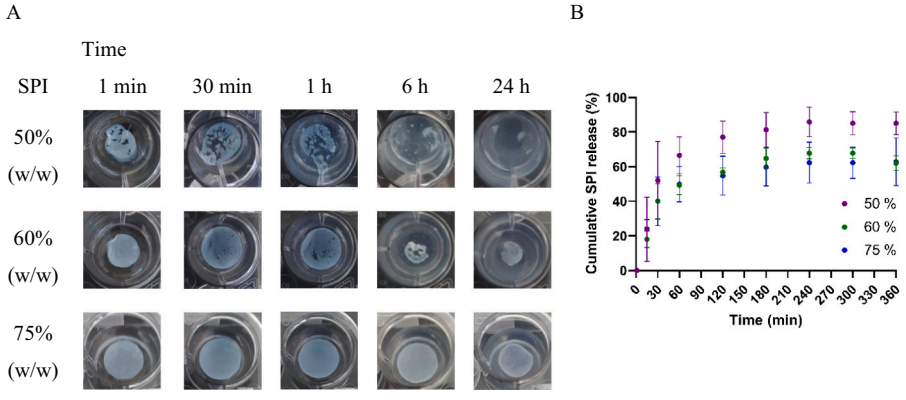

Fig. 7. The aqueous stability of electrospun SPI/PEO nanofibers depends on the SPI content. A) Representative images of 10 mm discs of electrospun SPI/PEO nanofibers with various relative content of SPI submerged into water for 24 h. $N = 2$. B) Cumulative release of SPI from electrospun SPI/PEO nanofibers with 50%, 60% and 75% (w/w) content of SPI. The results are normalized to the initial content of SPI in the nanofibers. N = 2, $n = 3$. For all, N represents the number of batches of nanofibers and n the number of samples analyzed from each batch. Results presented as mean ± standard deviation.

fabrication of safer materials made from proteins.

4. Conclusions

Biocompatible electrospun nanofibers with a high content of SPI (up to 75% (w/w) SPI) were fabricated with PEO as a *co*-spinning polymer, by an environmentally friendly method and water being the only solvent; thus avoiding any use of organic solvents, strong bases or surfactants. A thorough biophysical assessment and rheological profiling of SPI in water suggested that sonication of SPI improved the electrospinnability by disassembly of larger structures into smaller in the SPI suspension. The content of SPI in the nanofibers affected the morphology, brittleness and aqueous stability, which are key parameters for the future use of SPI-based nanofibers. The biocompatibility of the electrospun SPI/PEO nanofibers was demonstrated by exposure of human epithelial cell monolayers to the nanofibers without loss of cell viability. It is believed that the presented strategies can serve as a starting point for waterborne electrospinning of other proteins or protein isolates with the aim of producing more environmentally-friendly and safe nanofiber-based materials.

Funding sources

This work was supported by the VILLUM FONDEN for the Villum Young Investigator Grant "Protein superstructure as Smart Biomaterials (ProSmart)" 2018–2023 (project number: 19175), the University of Palermo (FFR – PROMETA), the Novo Nordisk Foundation, NNF20OC0065260, the Novo Nordisk Foundation Grand Challenge Program, NNF16OC0021948 and the Innovation Fund Denmark PROBIO, project-7076-00053B.

CRediT authorship contribution statement

Mai Bay Stie: Conceptualization, Formal analysis, Investigation, Methodology, Project administration, Visualization, Writing – original draft. **Kleopatra Kalouta:** Conceptualization, Formal analysis, Investigation, Methodology, Project administration, Visualization, Writing – original draft. **Cristiana Filipa Barreiro da Cunha:** Formal analysis, Investigation, Writing – review & editing. **Halimah Masood Feroze:** Investigation, Writing – review & editing. **Valeria Vetri:** Conceptualization, Funding acquisition, Methodology, Supervision, Project administration, Resources, Writing – review & editing. **Vito Foderà:** Conceptualization, Funding acquisition, Methodology, Supervision, Project administration, Resources, Writing – review & editing.

Declaration of Competing Interest

The authors declare no conflict of interest.

Data availability

Data will be made available on request.

Acknowledgement

We acknowledge the Core Facility for Integrated Microscopy (CFIM), Faculty of Health and Medical Sciences, University of Copenhagen. Sara Anselmo is acknowledged for help with microscopy imaging. Associate Professor Marco van de Weert is acknowledged for reviewing the manuscript and for providing useful comments and discussion on the subject.

Appendix A. Supplementary data

Supplementary data to this article can be found online at https://doi.org/10.1016/j.susmat.2022.e00519.

References

[1] 1 United Nations General Assembly, 70/1 Transforming Our World: The 2030 Agenda for Sustainable Development, 2015. A/RES/70/1.
[2] M. Maeda, K. Kadota, M. Kajihara, A. Sano, K. Fujioka, Sustained release of human growth hormone (HGH) from collagen film and evaluation of effect on wound healing in Db/Db mice, J. Control. Release 77 (3) (2001) 261–272, https://doi.org/10.1016/S0168-3659(01)00512-0.
[3] B. Yavuz, L. Chambre, K. Harrington, J. Kluge, L. Valenti, D.L. Kaplan, Silk fibroin microneedle patches for the sustained release of levonorgestrel, ACS Appl. Bio Mater. 3 (8) (2020) 5375–5382, https://doi.org/10.1021/acsabm.0c00671.
[4] B.A. Jones, D. Grace, R. Kock, S. Alonso, J. Rushton, M.Y. Said, D. McKeever, F. Mutua, J. Young, J. McDermott, D.U. Pfeiffer, Zoonosis emergence linked to agricultural intensification and environmental change, Proc. Natl. Acad. Sci. 110 (21) (2013) 8399–8404, https://doi.org/10.1073/pnas.1208059110.
[5] M.A. Asgar, A. Fazilah, N. Huda, R. Bhat, A.A. Karim, Nonmeat protein alternatives as meat extenders and meat analogs, Compr. Rev. Food Sci. Food Saf. 9 (5) (2010) 513–529, https://doi.org/10.1111/j.1541-4337.2010.00124.x.
[6] M.B. Stie, K. Kalouta, V. Vetri, V. Foderà, Protein materials as sustainable non- and minimally invasive strategies for biomedical applications, J. Control. Release 344 (2022) 12–25, https://doi.org/10.1016/j.jconrel.2022.02.016.
[7] S.S. Shidhaye, N.S. Saindane, S. Sutar, V. Kadam, Mucoadhesive bilayered patches for administration of sumatriptan succinate, AAPS PharmSciTech 9 (3) (2008) 909–916, https://doi.org/10.1208/s12249-008-9125-x.
[8] A.K.M.M. Alam, Q.T.H. Shubhra, Surface modified thin film from silk and gelatin for sustained drug release to heal wound, J. Mater. Chem. B 3 (31) (2015) 6473–6479, https://doi.org/10.1039/C5TB00920K.
[9] M. Rafat, F. Li, P. Fagerholm, N.S. Lagali, M.A. Watsky, R. Munger, T. Matsuura, M. Griffith, PEG-stabilized carbodiimide crosslinked collagen–chitosan hydrogels for corneal tissue engineering, Biomaterials 29 (29) (2008) 3960–3972, https://doi.org/10.1016/j.biomaterials.2008.06.017.
[10] K.-L. Mao, Z.-L. Fan, J.-D. Yuan, P.-P. Chen, J.-J. Yang, J. Xu, D.-L. ZhuGe, B.-H. Jin, Q.-Y. Zhu, B.-X. Shen, Y. Sohawon, Y.-Z. Zhao, H.-L. Xu, Skin-penetrating polymeric nanoparticles incorporated in silk fibroin hydrogel for topical delivery of curcumin to improve its therapeutic effect on psoriasis mouse model, Colloids Surf. B: Biointerfaces 160 (2017) 704–714, https://doi.org/10.1016/j.colsurfb.2017.10.029.
[11] N. Annabi, S.M. Mithieux, E.A. Boughton, A.J. Ruys, A.S. Weiss, F. Dehghani, Synthesis of highly porous crosslinked elastin hydrogels and their interaction with fibroblasts in vitro, Biomaterials 30 (27) (2009) 4550–4557, https://doi.org/10.1016/j.biomaterials.2009.05.014.
[12] X. Xu, L. Jiang, Z. Zhou, X. Wu, Y. Wang, Preparation and properties of electrospun soy protein isolate/polyethylene oxide nanofiber membranes, ACS Appl. Mater. Interfaces 4 (8) (2012) 4331–4337, https://doi.org/10.1021/am300991e.
[13] M.B. Stie, M. Corezzi, A.D. Juncos Bombin, F. Ajallouеian, E. Attrill, S. Pagliara, J. Jacobsen, I.S. Chronakis, H.M. Nielsen, V. Foderà, Waterborne electrospinning of α-lactalbumin generates tunable and biocompatible nanofibers for drug delivery, ACS Appl. Nano Mater. 3 (2) (2020) 1910–1921, https://doi.org/10.1021/acsanm.9b02557.
[14] M. Faccini, C. Vaquero, D. Amantia, Development of protective clothing against nanoparticle based on electrospun nanofibers, J. Nanomater. 2012 (2012) 1–9, https://doi.org/10.1155/2012/892894.
[15] M.B. Dickerson, A.A. Sierra, N.M. Bedford, W.J. Lyon, W.E. Gruner, P.A. Mirau, R. R. Naik, Keratin-based antimicrobial textiles, films, and nanofibers, J. Mater. Chem. B 1 (40) (2013) 5505–5514, https://doi.org/10.1039/C3TB20896F.
[16] K. Min, S. Kim, S. Kim, Silk protein nanofibers for highly efficient, eco-friendly, optically translucent, and multifunctional air filters, Sci. Rep. 8 (1) (2018) 9598, https://doi.org/10.1038/s41598-018-27917-w.
[17] B. Dhandayuthapani, R. Mallampati, D. Sriramulu, R.F. Dsouza, S. Valiyaveettil, PVA/gluten hybrid nanofibers for removal of nanoparticles from water, ACS Sustain. Chem. Eng. 2 (4) (2014) 1014–1021, https://doi.org/10.1021/sc500003k.
[18] Y. Tang, Y. Zhou, X. Lan, D. Huang, T. Luo, J. Ji, Z. Mafang, X. Miao, H. Wang, W. Wang, Electrospun gelatin nanofibers encapsulated with peppermint and chamomile essential oils as potential edible packaging, J. Agric. Food Chem. 67 (8) (2019) 2227–2234, https://doi.org/10.1021/acs.jafc.8b06226.
[19] Y.E. Arslan, T. Sezgin Arslan, B. Derkus, E. Emregul, K.C. Emregul, Fabrication of human hair keratin/jellyfish collagen/eggshell-derived hydroxyapatite osteoinductive biocomposite scaffolds for bone tissue engineering: from waste to regenerative medicine products, Colloids Surf. B: Biointerfaces 154 (2017) 160–170, https://doi.org/10.1016/j.colsurfb.2017.03.034.
[20] K. Kalouta, M.B. Stie, C. Janfelt, I.S. Chronakis, J. Jacobsen, H. Mørck Nielsen, V. Foderà, Electrospun α-lactalbumin nanofibers for site-specific and fast-onset delivery of nicotine in the oral cavity: an *in vitro*, *ex vivo*, and tissue spatial distribution study, Mol. Pharm. 17 (11) (2020) 4189–4200, https://doi.org/10.1021/acs.molpharmaceut.0c00642.
[21] A. Akhmetova, A. Heinz, Electrospinning proteins for wound healing purposes: opportunities and challenges, Pharmaceutics (2021), https://doi.org/10.3390/pharmaceutics13010004.
[22] I.S. Chronakis, Micro-/nano-fibers by electrospinning technology, in: Micro-Manufacturing Engineering and Technology, Elsevier, 2010, pp. 264–286, https://doi.org/10.1016/B978-0-8155-1545-6.00016-8.
[23] A.C. Mendes, K. Stephansen, I.S. Chronakis, Electrospinning of food proteins and polysaccharides, Food Hydrocoll. 68 (2017) 53–68, https://doi.org/10.1016/j.foodhyd.2016.10.022.

[24] J. Avossa, G. Herwig, C. Toncelli, F. Itel, R.M. Rossi, Electrospinning based on benign solvents: current definitions, implications and strategies, Green Chem. 24 (6) (2022) 2347–2375, https://doi.org/10.1039/D1GC04252A.
[25] E. Schoolaert, P. Ryckx, J. Geltmeyer, S. Maji, P.H.M. Van Steenberge, D. R. D'hooge, R. Hoogenboom, K. De Clerck, Waterborne electrospinning of poly(N-isopropylacrylamide) by control of environmental parameters, ACS Appl. Mater. Interfaces 9 (28) (2017) 24100–24110, https://doi.org/10.1021/acsami.7b05074.
[26] O. Flynn, D. Timothy, S.A. Hogan, D.F.M. Daly, J.A. O Mahony, N.A. McCarthy, Rheological and solubility properties of soy protein isolate, Molecules 26 (10) (2021) 3015, https://doi.org/10.3390/molecules26103015.
[27] S.T. Sullivan, C. Tang, A. Kennedy, S. Talwar, S.A. Khan, Electrospinning and heat treatment of whey protein nanofibers, Food Hydrocoll. 35 (2014) 36–50, https://doi.org/10.1016/j.foodhyd.2013.07.023.
[28] P. Singh, R. Kumar, S.N. Sabapathy, A.S. Bawa, Functional and edible uses of soy protein products, Compr. Rev. Food Sci. Food Saf. 7 (1) (2008) 14–28, https://doi.org/10.1111/j.1541-4337.2007.00025.x.
[29] D. Fukushima, Soy proteins, in: Handbook of Food Proteins, Elsevier, 2011, pp. 210–232, https://doi.org/10.1533/9780857093639.210.
[30] N. Varshney, A.K. Sahi, S. Poddar, S.K. Mahto, Soy protein isolate supplemented silk fibroin nanofibers for skin tissue regeneration: fabrication and characterization, Int. J. Biol. Macromol. 160 (2020) 112–127, https://doi.org/10.1016/j.ijbiomac.2020.05.090.
[31] M. Thirugnanaselvam, N. Gobi, S. Arun Karthick, SPI/PEO blended electrospun martrix for wound healing, Fibers Polym. 14 (6) (2013) 965–969, https://doi.org/10.1007/s12221-013-0965-y.
[32] D. Gutschmidt, R.S. Hazra, X. Zhou, X. Xu, M. Sabzi, L. Jiang, Electrospun, sepiolite-loaded poly(vinyl alcohol)/soy protein isolate nanofibers: preparation, characterization, and their drug release behavior, Int. J. Pharm. 594 (2021), 120172, https://doi.org/10.1016/j.ijpharm.2020.120172.
[33] R. Wongkanya, P. Chuysinuan, C. Pengsuk, S. Techasakul, K. Lirdprapamongkol, J. Svasti, P. Nooeaid, Electrospinning of alginate/soy protein isolated nanofibers and their release characteristics for biomedical applications, J. Sci. Adv. Mater. Devices 2 (3) (2017) 309–316, https://doi.org/10.1016/j.jsamd.2017.05.010.
[34] K. Ramji, R.N. Shah, Electrospun soy protein nanofiber scaffolds for tissue regeneration, J. Biomater. Appl. 29 (3) (2014) 411–422, https://doi.org/10.1177/0885328214530765.
[35] D. Cho, A.N. Netravali, Y.L. Joo, Mechanical properties and biodegradability of electrospun soy protein isolate/PVA hybrid nanofibers, Polym. Degrad. Stab. 97 (5) (2012) 747–754, https://doi.org/10.1016/j.polymdegradstab. 2012.02.007.
[36] D. Cho, O. Nnadi, A. Netravali, Y.L. Joo, Electrospun hybrid soy protein/PVA fibers, Macromol. Mater. Eng. 295 (8) (2010) 763–773, https://doi.org/10.1002/mame.201000161.
[37] A. Barth, C. Zscherp, What vibrations tell about proteins, Q. Rev. Biophys. 35 (4) (2002) 369–430, https://doi.org/10.1017/S0033583502003815.
[38] F. Piccirilli, G. Schirò, V. Vetri, S. Lupi, A. Perucchi, V. Militello, Decoding vibrational states of concanavalin a amyloid fibrils, Biophys. Chem. 199 (2015) 17–24, https://doi.org/10.1016/j.bpc.2015.02.007.
[39] D. Mailley, A. Hébraud, G. Schlatter, A review on the impact of humidity during electrospinning: from the nanofiber structure engineering to the applications, Macromol. Mater. Eng. 306 (7) (2021), https://doi.org/10.1002/mame.202100115, 2100115.
[40] J. Pelipenko, J. Kristl, B. Janković, S. Baumgartner, P. Kocbek, The impact of relative humidity during electrospinning on the morphology and mechanical properties of nanofibers, Int. J. Pharm. 456 (1) (2013) 125–134, https://doi.org/10.1016/j.ijpharm.2013.07.078.
[41] T.D. O'Flynn, S.A. Hogan, D.F.M. Daly, J.A. O'Mahony, N.A. McCarthy, Rheological and solubility properties of soy protein isolate, Molecules (2021), https://doi.org/10.3390/molecules26103015.
[42] A. Kamada, M. Rodriguez-Garcia, F.S. Ruggeri, Y. Shen, A. Levin, T.P.J. Knowles, Controlled self-assembly of plant proteins into high-performance multifunctional nanostructured films, Nat. Commun. 12 (1) (2021) 3529, https://doi.org/10.1038/s41467-021-23813-6.
[43] G. Yildiz, J. Andrade, N.E. Engeseth, H. Feng, Functionalizing soy protein nano-aggregates with pH-shifting and mano-thermo-sonication, J. Colloid Interface Sci. 505 (2017) 836–846, https://doi.org/10.1016/j.jcis.2017.06.088.
[44] Q. Liu, R. Geng, J. Zhao, Q. Chen, B. Kong, Structural and gel textural properties of soy protein isolate when subjected to extreme acid pH-shifting and mild heating processes, J. Agric. Food Chem. 63 (19) (2015) 4853–4861, https://doi.org/10.1021/acs.jafc.5b01331.
[45] A. Ghisaidoobe, S. Chung, Intrinsic tryptophan fluorescence in the detection and analysis of proteins: a focus on Förster resonance energy transfer techniques, Int. J. Mol. Sci. 15 (12) (2014) 22518–22538, https://doi.org/10.3390/ijms151222518.
[46] Y. Chen, M.D. Barkley, Toward understanding tryptophan fluorescence in proteins, Biochemistry 37 (28) (1998) 9976–9982, https://doi.org/10.1021/bi980274n.
[47] P. Shen, F. Zhou, Y. Zhang, D. Yuan, Q. Zhao, M. Zhao, Formation and characterization of soy protein nanoparticles by controlled partial enzymatic hydrolysis, Food Hydrocoll. 105 (2020), 105844, https://doi.org/10.1016/j.foodhyd.2020.105844.
[48] L. Zheng, Z. Wang, Y. Kong, Z. Ma, C. Wu, J.M. Regenstein, F. Teng, Y. Li, Different commercial soy protein isolates and the characteristics of Chiba tofu, Food Hydrocoll. 110 (2021), 106115, https://doi.org/10.1016/j.foodhyd.2020.106115.
[49] H. Yang, S. Yang, J. Kong, A. Dong, S. Yu, Obtaining information about protein secondary structures in aqueous solution using Fourier transform IR spectroscopy, Nat. Protoc. 10 (3) (2015) 382–396, https://doi.org/10.1038/nprot.2015.024.
[50] G. Zandomeneghi, M.R.H. Krebs, M.G. McCammon, M. Fändrich, FTIR reveals structural differences between native beta-sheet proteins and amyloid fibrils, Protein Sci. 13 (12) (2004) 3314–3321, https://doi.org/10.1110/ps.041024904.
[51] K. Li, S. Jin, Y. Han, J. Li, H. Chen, Improvement in functional properties of soy protein isolate-based film by cellulose nanocrystal–graphene artificial nacre nanocomposite, Polymers (2017), https://doi.org/10.3390/polym9080321.
[52] F. Bonnier, H. Blasco, C. Wasselet, G. Brachet, R. Respaud, L.F.C.S. Carvalho, D. Bertrand, M.J. Baker, H.J. Byrne, I. Chourpa, Ultra-filtration of human serum for improved quantitative analysis of low molecular weight biomarkers using ATR-IR spectroscopy, Analyst 142 (8) (2017) 1285–1298, https://doi.org/10.1039/C6AN01888B.
[53] M.B. Stie, M. Jones, H.O. Sørensen, J. Jacobsen, I.S. Chronakis, H.M. Nielsen, Acids 'generally recognized as safe' affect morphology and biocompatibility of electrospun chitosan/polyethylene oxide nanofibers, Carbohydr. Polym. 215 (2019) 253–262, https://doi.org/10.1016/j.carbpol.2019.03.061.
[54] J.-F. Su, Z. Huang, C.-M. Yang, X.-Y. Yuan, Properties of soy protein isolate/poly (vinyl alcohol) blend "green" films: compatibility, mechanical properties, and thermal stability, J. Appl. Polym. Sci. 110 (6) (2008) 3706–3716, https://doi.org/10.1002/app.28979.
[55] C. Chong, Y. Wang, A. Fathi, R. Parungao, P.K. Maitz, Z. Li, Skin wound repair: results of a pre-clinical study to evaluate electropsun collagen–elastin–PCL scaffolds as dermal substitutes, Burns 45 (7) (2019) 1639–1648, https://doi.org/10.1016/j.burns.2019.04.014.
[56] H. Samadian, S. Zamiri, A. Ehterami, S. Farzamfar, A. Vaez, H. Khastar, M. Alam, A. Ai, H. Derakhshankhah, Z. Allahyari, A. Goodarzi, M. Salehi, Electrospun cellulose acetate/gelatin nanofibrous wound dressing containing berberine for diabetic foot ulcer healing: *in vitro* and *in vivo* studies, Sci. Rep. 10 (1) (2020) 8312, https://doi.org/10.1038/s41598-020-65268-7.
[57] S. Amadori, P. Torricelli, K. Rubini, M. Fini, S. Panzavolta, A. Bigi, Effect of sterilization and crosslinking on gelatin films, J. Mater. Sci. Mater. Med. 26 (2) (2015) 69, https://doi.org/10.1007/s10856-015-5396-4.
[58] J.E. Gough, C.A. Scotchford, S. Downes, Cytotoxicity of glutaraldehyde crosslinked collagen/poly(vinyl alcohol) films is by the mechanism of apoptosis, J. Biomed. Mater. Res. 61 (1) (2002) 121–130, https://doi.org/10.1002/jbm.10145.